Biosensors and Bioelectronics 26 (2010) 822–827

Contents lists available at ScienceDirect

Biosensors and Bioelectronics

journal homepage: www.elsevier.com/locate/bios

Significance of the pH-induced conformational changes in the structure of C-reactive protein measured by dual polarization interferometry

Bor-Ching Sheu[a,*], Yun-Han Lin[b], Chih-Chen Lin[b], Adam Shih-Yuan Lee[b], Wen-Chun Chang[a], Jung-Hsin Wu[b], Jui-Chang Tsai[c], Shiming Lin[c,**]

[a] Department of Obstetrics and Gynecology, College of Medicine and the Hospital, National Taiwan University, Taipei, Taiwan
[b] Department of Chemistry, Tamkang University, Tamsui, Taiwan
[c] Centre for Optoelectronic Biomedicine, National Taiwan University, Taipei, Taiwan

ARTICLE INFO

Article history:
Received 23 February 2010
Received in revised form 11 May 2010
Accepted 1 June 2010
Available online 15 June 2010

Keywords:
C-reactive protein
Dual polarization interferometry
pH
Cardiovascular disease

ABSTRACT

Emerging evidence indicates that the conformation of C-reactive protein (CRP) plays important roles in human inflammation and cardiovascular disease (CVD). The different conformations in the structure of CRP under different pH conditions remain an important issue to be investigated for explaining various functions of CRP under certain physiologic and pathologic conditions. We directly measured the pH-induced conformational changes in the structure of CRP by dual polarization interferometry (DPI). The CRP was attached to an aldehyde-functionalized DPI sensor chip at a concentration of 50 μg/ml, and attained 2.019 ng/mm^2 to form a surface coverage with a 1.71×10^{-14} mol/mm^2 CRP monolayer. A pentagonal structure with an average monolayer thickness value of 5.70 ± 0.12 nm and a layer density of 0.374 ± 0.058 g/cm^2 was obtained at pH 7.0. Moreover, the DPI biosensor signals directly reflected the considerable structural parameters and phenomena of conformational changes of CRP in a pH range of 2.0–10.0. The results obtained showed that the pentameric structure of CRP might dissociated into monomers or monomer aggregates as the pH shifts toward both acidic and alkaline conditions, but only partial rearrangements of CRP subunits might occur at extremely acidic physiological conditions. Considering the proinflammatory effect and subclinical chronic inflammation, pH-induced conformational changes in the structure of CRP between monomeric and pentameric formations may strongly relate to vascular atherosclerosis and subsequent CVD.

1. Introduction

The hepatocyte-derived acute-phase reactant C-reactive protein (CRP) has been intensely investigated for its probable role in the pathogenesis of a variety of human diseases. CRP is known as a human blood serum marker for infections and inflammatory processes. The blood serum concentration of CRP can increase 1000-fold during acute inflammatory stress (Blake et al., 2003). The pentagonal structure of doughnut-shaped C-reactive protein has been determined by us using an atomic force microscope (AFM) and a dual polarization interferometric biosensor (Lin et al., 2006a). These types of structures have been described as "pentraxins", and every subunit exerts a phosphocholine binding site (Mazer and Rabbani, 2004; Pepys and Hirschfield, 2003). Clinically, elevated serum CRP level is proposed to be a significant and independent indicator of possible future cardiovascular disease (CVD) (Mazer and Rabbani, 2004; Pepys and Hirschfield, 2003). Generally, low-grade inflammation is characteristic of metabolic syndrome (Devaraj et al., 2009). Low concentrations of CRP circulating in the absence of an overt infective or inflammatory episode are proposed as a potential causal factor of CVD (Casas et al., 2008). Associated clinical researches show that high acute-phase CRP concentrations can influence the severity of ischemic tissue damage and the subsequent poor prognosis (Nakou et al., 2008). Moreover, development of high-sensitivity CRP (hsCRP) assays that can measure low concentrations of circulating CRP has been utilized for the plausible prediction of therapeutically targeted CVD (Araujo et al., 2009; Musunuru et al., 2008; Hingorani et al., 2009). However, despite the emerging evidence suggesting the proatherogenic role of CRP in human CVD, the responsible mechanism of CRP in related pathogenesis has not been clearly defined (Hingorani et al., 2009).

The pathophysiologic roles of CRP in human disease conditions largely depend on its structure, which is proposed to originate from the considerable conformational heterogeneity of the CRP molecule (Boncler and Watala, 2009; Hage and Szalai, 2009). Two CRP

* Corresponding author. Tel.: +886 2 23123456x71508; fax: +886 2 27092570.
** Corresponding author at: Centre for Optoelectronic Biomedicine, National Taiwan University, College of Medicine, No.1, Section 1, Jen-Ai Road, Taipei 100, Taiwan. Tel.: +886 2 23123456x8458; fax: +886 2 23949125.
E-mail addresses: bcsheu@ntu.edu.tw (B.-C. Sheu), til@ntu.edu.tw (S. Lin).

0956-5663/$ – see front matter © 2010 Elsevier B.V. All rights reserved.
doi:10.1016/j.bios.2010.06.001

isoforms, the native pentameric and the modified monomeric isoforms, differ substantially in their physiological functions (Boncler and Watala, 2009). Native pentameric CRP must undergo structural dissociation to form monomeric subunits before promoting a proinflammatory reaction, and patients with more monomeric CRP have an increased tendency for adverse CVD (Khreiss et al., 2004). Although many clinical studies link the associations of CRP and inflammation and CVD, the CRP conformational changes, especially under extreme pH conditions within inflammatory or CVD tissue milieu, remain an issue to be investigated (Verma et al., 2004). Under certain physiologic and pathologic conditions, the microenvironment of local inflammatory tissue will have an extremely wide range of pH (Verma et al., 2004). For example, the normal pH value of human vagina is below pH 4, and the pH value will shift during inflammation induced by bacterial vaginitis. The pH value of gastric acid secretion may be below pH 2 in acute and chronic inflammatory gastritis. In acute pancreatitis, the pH value of local inflammatory tissue will rise over pH 10 when the tissue is digested by the alkaloid pancreatic enzymes.

A variety of biosensors have been developed in the last decade to examined surface properties of adsorbed protein layers at sensor surfaces. Some of the more sensitive detection methods rely on evanescent wave techniques, e.g., surface plasmon resonance (SPR) and dual polarization interferometry (DPI) phenomenon. DPI sensor has been introduced for the evaluation of conformational changes in the protein structure (Swann et al., 2004). By addressing the waveguide structure with alternate polarizations, one can determine the optogeometrical properties (density and thickness) of adsorbed protein layers at the sensor (solid)–liquid interface. Also, SPR biosensors have been widely used to study conformational changes of biomolecules, and they have been utilized to study conformational changes of CRP layer (Meyer et al., 2006). The advantage of the DPI technique is that it allows the calculation of the interaction stoichiometry and also allows the discrimination between surface loss during binding that were not discriminated by SPR. However, SPR, due to the spot sensing in this technique, is more accurate than DPI when studying initial kinetics of adsorption to surfaces.

The present study used a DPI biosensor to provide a real-time and accurate approach to characterize a CRP monolayer under different pH conditions. The considerable structural parameters, including the pH-induced conformational changes of the homopentamer CRP, were determined on the aminated-functionalized surface.

2. Materials and methods

2.1. Setting of dual polarization interferometry

The *Ana*Light® Bio200 DPI biosensor (Farfield Sensors Ltd., Manchester, UK) was applied in all experiments in this study. The well-known Young's interference experiment is the fundamental theory of dual polarization that offers an extra dimension at the chip surface. The optical component of the *Ana*Light® Bio200 DPI biosensor is a helium neon laser ($\lambda = 632.8$ nm) which illuminates the end facet of the chip with a line image applied with a Powell lens. The state of polarization of the input beam is switched between transverse electric (TE) and transverse magnetic (TM) using a ferroelectric liquid crystal (FLC) 1/2 wave plate at typical frequencies of 50 Hz by the digital signal processing (DSP) chip. The fluidic handling system associated with the instrument utilizes conventional high performance liquid chromatography components, a reciprocating pump (Kanuer D-14163, Germany) to provide motive force, a six-port valve (Rheodyne 9725i, USA) to inject the desired materials, and a diverter valve (Anachem V-101T, USA) to enable either or simultaneously both of the two sensitive channels on the sensor chip to be addressed.

2.2. Quantitative analysis of dual polarization interferometry

Quantitative analysis data of the film thickness and density at the silica-based surface were obtained under light propagation into the waveguide. The changes in the two polarizations, TM and TE, were attributed to two parameters to calculate the refractive index and thickness of each layer via the Maxwell equation. DPI measured the structure of a protein in the subatomic resolutions (typically to 0.01 nm) in protein layer thickness in real time.

2.3. Amination of the DPI sensor chip

An unmodified DPI sensor chip (*Ana*Chip™, Farfield Sensors Ltd., Manchester, UK) was subjected to a series of silanization methods to provide an amine-functionalized sensor surface as previously mentioned (Lin et al., 2006a,b). The sensor chip was first sonicated in acetone for 3 min to remove oil and particles, and then bathed in hot piranha acid (H_2O_2/H_2SO_4, 1:3, v/v) for at least 10 min to remove organic impurities and most contaminants. The hydroxyl surface was silanized with a 10% solution of 3-aminopropyltriethoxysilane (3-APTES) (Sigma–Aldrich, USA) in 5% ethanol/95% water at room temperature for 2 h. The sensor chip was then rinsed with a 5% ethanol/95% water solution, followed by air drying for 15–30 min.

2.4. Immobilization of CRP monolayer on DPI biosensor

All experimental conditions for CRP immobilization were established in accordance with our previous study (Lin et al., 2006a,b). In brief, the sensor chip with amine functions via covalent binding to the surface was mounted in a DPI biosensor. The internal temperature of the instrument was set at 20 °C (±0.002 °C), with the standard fluidic system as supplied. The PBS buffer (pH 7.0) flowed over the surface until the baseline response stabilized. The flow rate was less 50 μl/min to prevent surface brushing. Ethanol 80% and deionized water with known refractive indices (RI) were respectively poured over the surface at 50 μl/min to calibrate the sensor chip. The thickness and RI of the waveguide sensor layer were all resolved before adding the sample. Glutaraldehyde 4% (Sigma–Aldrich, USA) in H_2O was injected for 2 min, and then stopped. The incubation of glutaraldehyde on the surface for 20 min activated the aminated surface to an aldehyde-functionalized surface. Different concentrations of CRP (Sigma–Aldrich, I5154, Saint Louis, USA) in PBS buffer containing 50 μg/ml calcium chloride were then prepared for the experiment. The flow rate was then reduced to 20 μl/min to construct a unique CRP monolayer. CRP was injected at a concentration of 100 μg/ml over the sensor chip and allowed to interact freely with the aldehyde-functionalized surface for 10 min. TM/TE data was then acquired from various concentrations (5, 10, 20, 50, 100 μg/ml) of CRP.

2.5. pH-induced conformational changes in the structure of CRP

After the immobilization of CRP, 100 μl of each different pH solution (Sigma–Aldrich, USA) was injected to induce a CRP conformational change. The CRP monolayer was exposed to various buffer solutions including 0.1 M glycine–HCl buffer (pH 2.0), 0.1 M acetate buffer (pH 4.0), 0.1 M citrate–phosphate buffer (pH 6.0), 0.1 M Tris–HCl buffer (pH 8.0), and 0.1 M carbonate–bicarbonate buffer (pH 10.0) for 5 min. The flow rates were all controlled at 20 μl/min. The running buffer (pH 7.0) was then switched to PBS and poured over the surface for 10 min to attain equilibrium. Further reversible arrangement and structural parameters of CRP were

determined from the TM/TE data acquired under the solid-liquid surface.

3. Results and discussion

3.1. Calibration of the immobilized CRP monolayer of various concentrations

The initial calibration procedure was applied before the monolayer characterization of CRP. The injection of 80% ethanol with a known RI of 1.3658 that did not affect the layer on the aminated surface enabled the waveguide characteristics to be precisely determined. The subsequent deionozed water injection enabled accurate determination of the RI of the PBS running buffer at 1.335 (±0.001). With the formation of a –CH=N-bond, the increase of 0.54 nm in the aldehyde activated surface provided a biologically active surface for CRP immobilization (Fig. 1). Both the TM and TE phase responses obtained from the CRP immobilization experiment are shown in Fig. 1A. The changes in the phases referred to as TM and TE in the sensorgram were followed as a function of time and resolved into the layer thickness and density changes.

3.2. Characterization of the CRP monolayer

The protein layer density (CRP monolayer in g/cm^3) was obtained from the RI using the appropriate RI increment values. It is generally accepted from ellipsometric measurements that densely physisorbed protein layers, in an aqueous environment with an RI of 1.333, have an RI of 1.465 (Arwin, 2000; Wen and Arakawa, 2000). This could give a density of 0.71 g/cm^3 using an average value for the RI increment of 0.186. Given these values, the density of the protein [CRP] layer could be found from the measured refractive index of the CRP layer, n, under the assumption of additivity of the constituents, as follows: $\rho_L = (n_L - n_s)/(n_p - n_s) \times \rho_p$, where ρ_L is the density of the layer (in g/cm^3), ρ_p is the density of pure protein (in g/cm^3), n_L is the measured RI of the layer, n_s is the measured RI of the bulk solution, and n_p is the RI of the pure protein. Also, $\rho_L = (n_L - n_s)/(dn/dc)$, where dn/dc is the RI increment, which in the case of proteins is 0.186. Therefore the layer density and thickness of different CRP concentrations could be determined, as shown in Fig. 1B.

The mass loading per unit area, which is simply the product of the measured layer thickness and calculated layer density (derived from the RI), is as follows: $m_L = \rho_L \times d_L$, where m_L is the mass per unit area, ρ_L is the layer density, and dL is the layer thickness. When the thickness is expressed in nanometers and the density is expressed in grams per centimeter cubed, the result is expressed in ng/mm^2. The layer characteristics in terms of mass (surface concentration) of the CRP layer obtained are shown in Fig. 1C.

3.3. Concentrations of CRP influence the immobilization layer thickness

To prepare a full CRP monolayer for further determination of the pH-induced conformational change at the solid–liquid interface, we varied the concentration of CRP added to the glutaraldehyde-functionalized sensor surface (Fig. 2). Fig. 2A shows the resolved layer thickness and RI versus the concentration of CRP added to the sensor surface. The data showed that as the CRP concentration increased, the adsorbed layer thickness increased and the RI decreased. Before immobilization with the 20 μg/ml concentration of CRP, there was a sharp increase in the thickness and a decrease in the RI. The layer thickness tended to reach a stable stage after immobilization with a CRP concentration of 50 μg/ml to increase by 5.16 ± 0.12 nm. Since that atomic force microscopy (Lin et al., 2006a) studies showed that CRP is a pentagonal doughnut-shaped molecule, and the overall dimensions of the CRP pentamer are about 11.13 ± 1.47 nm for the outside diameter with a central pore diameter of 3.52 ± 0.42 nm, which are respectively close to those (102 Å in outside diameter and 30 Å in pore diameter) previously obtained from the structure of CRP determined by X-ray crystallography (Shrive et al., 1996). Therefore, the observed thickness

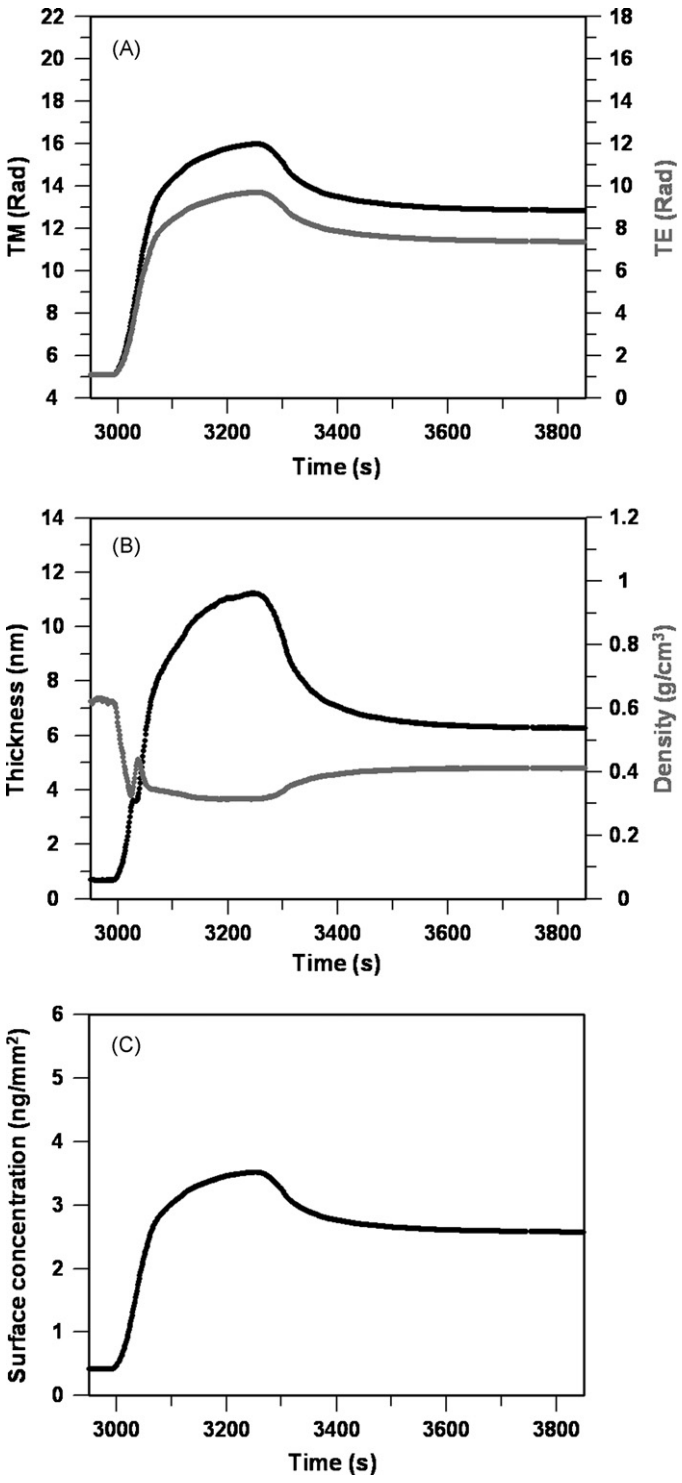

Fig. 1. Immobilization of CRP on a glutaldehyde-functionalized sensor chip surface as shown by (A) the measured TM (black line) and TE (gray line) phase changes, (B) together with the resolved layer thickness (black line), density (gray line), and (C) mass loading (surface concentration).

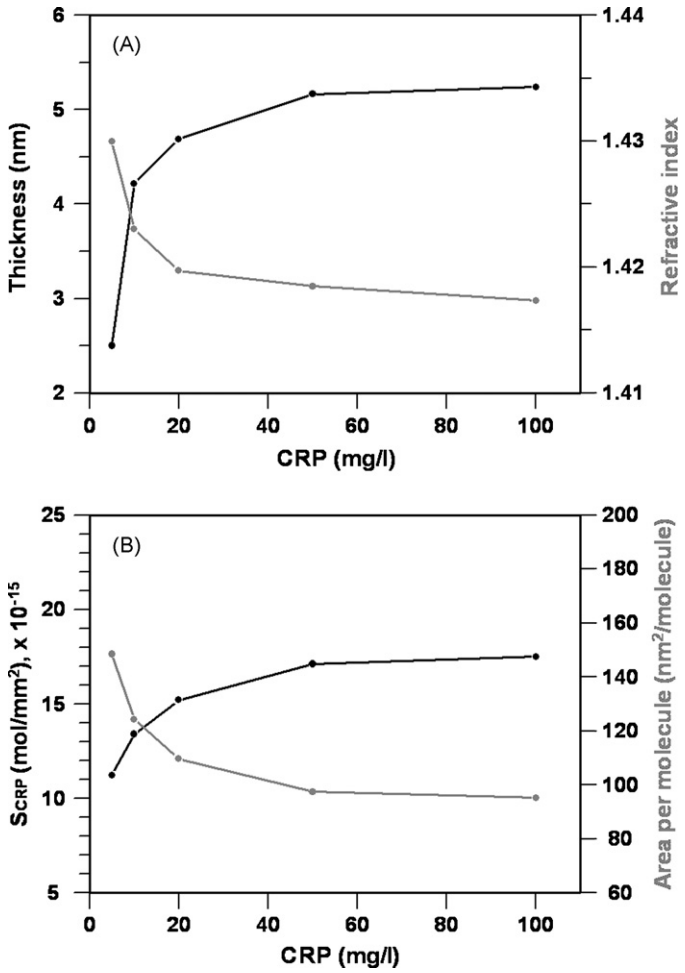

Fig. 2. Addition of various concentrations (5, 10, 20, 50, 100 μg/ml) of CRP onto a glutaldehyde-functionalized DPI sensor chip are shown as (A) the resolved layer thickness (black line) and refractive index (gray line) together with the transformed surface concentration (S_{CRP}) of the CRP layer (black line) and the area per CRP molecule (gray line). (B) The S_{CRP} increased up to a maximum binding capacity (approximately 1.71×10^{-14} mol/mm^2 or 97.4 nm^2/molecule) and then leveled off.

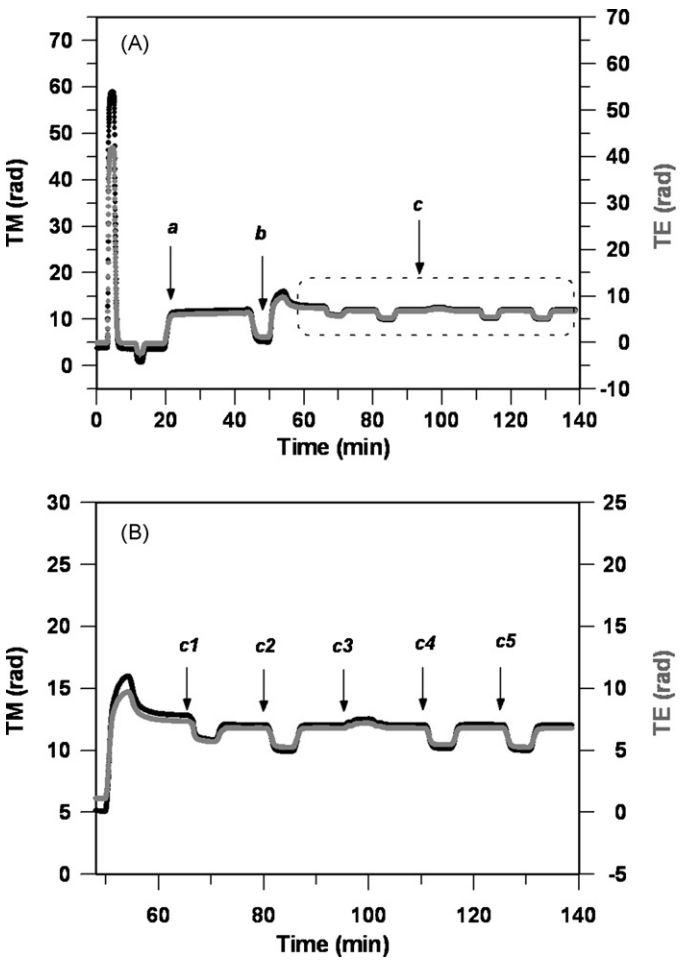

Fig. 3. CRP conformational changes in different pH solutions. (A) Raw phase data for the immobilization of CRP on a dual-waveguide sensor surface (black line denotes the TM response and dotted line denotes the TE response). Point a shows the addition of 4% glutaraldehyde to activate the aminated surface, point b shows the CRP immobilization, and point c shows the injection of various pH buffer solutions. (B) Phase changed data in radius (rad) with different pH solutions, points c1, c2, c3, c4, and c5 show 0.1 M glycine–HCl (pH 2.0), 0.1 M acetate (pH 4.0), 0.1 M citrate–phosphate (pH 6.0), 0.1 M Tris–HCl (pH 8.0), and 0.1 M carbonate–bicarbonate (pH 10.0) buffer solutions, respectively over the sensor surface.

increase of approximately 5.20 nm was attributed to the formation of a "partial" monolayer of protein immobilized on the sensor surface.

3.4. Determine the mass loading of CRP and surface coverage per molecule

The mass loading (surface concentration) of CRP, m_{CRP} (in ng/mm^2), was resolved from $m_{CRP} = \rho_{CRP} \times d_{CRP}$, where ρ_{CRP} was the density of the CRP molecular layer (in g/cm^3), and d_{CRP} was the thickness of the deposited CRP molecular layer. The area per CRP molecule of surface coverage S_{CRP} (in mol/mm^2), was obtained from $S_{CRP} = (m_{CRP}/M_{CRP})$, where M_{CRP} is the average CRP molecular mass (~118 kDa). Fig. 3 B shows the area per CRP molecule of surface coverage versus the concentration of CRP added to the sensor surface. Information on the area per molecule was calculated as follows: area per molecule = $1/(S_{CRP} \times$ Avogadro's number, $6.02 \times 10^{23})$. This determines whether a monolayer or multilayer is present. When the area per molecule was significantly lower than the theoretical saturated area per molecule, the structure was likely to be multilayer in nature. Here, the 'theoretical' saturated monolayer area per CRP molecule was estimated to be about 74.6 nm^2 (assuming a circular structure, the area $\pi \times$ [(outer diameter/2)^2 − (central pore diameter/2)^2].

As shown in Fig. 2B, surface coverage of CRP of 1.52×10^{-14} mol/mm^2 was observed at the 20 μg/ml CRP concentration, which was equivalent to an area per CRP molecule of 109.7 nm^2. Given that this figure was greater than the 'theoretical' saturated area per molecule (74.06 nm^2/molecule), the most likely surface structure would be a 'partial' monolayer coverage. With the concentration of 100 μg/ml, the CRP surface concentration (S_{CRP}) increased up to a maximum mass loading (approximately 1.75×10^{-14} mol/mm^2) and then leveled off. This behavior conforms to standard Langmuir isotherm characteristics. For example, with the 50 μg/ml CRP concentration, a surface coverage of CRP of 1.71×10^{-14} mol/mm^2 was observed, which could be equivalent to an area per CRP molecule of 97.4 nm^2. With a value of 95.2 nm^2 for the 100 μg/ml concentration. On the other hand, a typical self-assembled monolayer with a mass loading of approximately 2 ng/mm^2 was reported as compatible with 2.019 ng/mm^2 at a 50 μg/ml CRP concentration (Davis and Higson, 2005). Therefore, the CRP molecular dimensions of ultrathin film were employed in the determination of pH-induced conformational changes of CRP in the following sections.

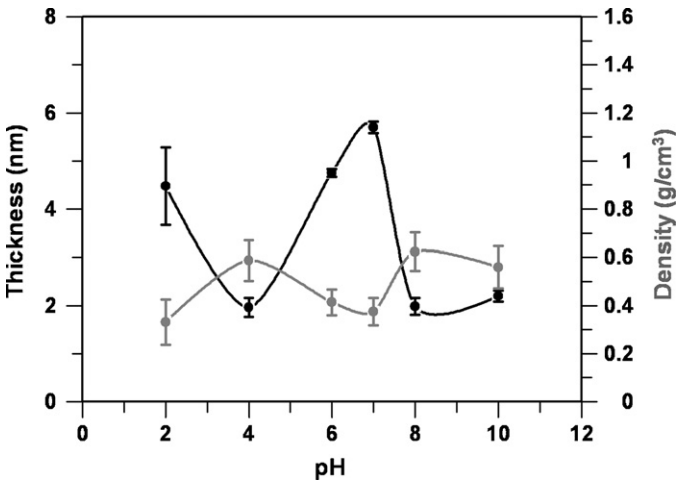

Fig. 4. The structural parameters of thickness (nm) and density (g/cm^3) of the CRP monolayer at the solid/liquid interface are characterized under different pH environments.

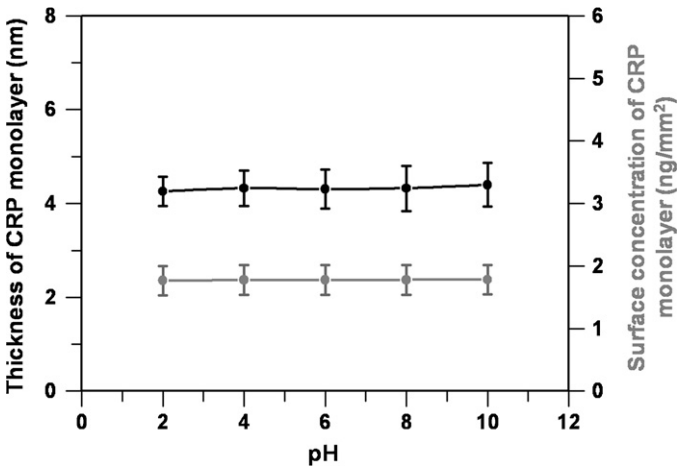

Fig. 5. Comparison of the thickness (nm) and surface concentration (ng/mm^2) of CRP monolayer indicate that the CRP retains a stable pentameric conformation after changes with solutions at different pHs (pH 2.0, pH 4.0, pH 6.0, pH 8.0, and pH 10.0).

3.5. CRP in different pH solutions

The immobilization of CRP was accompanied by a surface concentration of 1.71×10^{-14} mol/mm^2. An area per CRP molecule of 97.4 nm^2 was obtained to provide a stable CRP conformational state on a dual-waveguide sensor chip surface under physiological pH 7.0. Then, various pH buffer solutions were transported by diffusion and flowed over the sensor surface to react with the immobilized CRP. The pH-induced conformational changes all occurred on the aldehyde-functionalized sensor surface (Fig. 3). Fig. 3A shows that the DPI sensor monitored the responses in the TM and TE modes in all experimental steps, including: (1) the aldehyde surface functionalization process (point a), (2) the immobilization of CRP on the sensor chip (point b), and (3) the injection of various pH buffer solutions to provide different environments (point c). Changes in the TM/TE phase data in radians (rad) were resolved in term of the density and thickness of the CRP layer, as described above. Direct observation of CRP conformation showed an average thickness of 5.70 ± 0.12 nm and a layer density of 0.374 ± 0.058 g/cm^3 with the 50 μg/ml CRP concentration. This was followed by 0.1 M glycine–HCl buffer (pH 2.0, point c1), 0.1 M acetate buffer (pH 4.0, point c2), 0.1 M citrate–phosphate buffer (pH 6.0, point c3), 0.1 M Tris–HCl buffer (pH 8.0, point c4), and 0.1 M carbonate–bicarbonate buffer (pH 10.0, point c5) over the sensor surface, as shown in Fig. 3B. Significantly, the changes of TM/TE at pH 6.0 were smaller than those at other pH environments in the sensorgram. The clear decreases in TM/TE changes reached a range of 1.8–2.2 at pH 4.0, 8.0, and 10.0.

3.6. CRP in acidic pH conditions

The isoelectric point (p*I*), pH 6.3 ± 0.2, was based on the titration curve of native CRP (Laurent et al., 1983). The CRP was resolved into a thickness of 4.75 ± 0.08 nm and layer density of 0.413 ± 0.053 g/cm^3 at pH 6.0, as shown in Fig. 4. The CRP was resolved into a thickness of 1.96 ± 0.20 nm and a layer density of 0.587 ± 0.084 g/cm^3 at pH 4.0. The 3.74 nm decrease in thickness and 0.213 g/cm^3 increase in layer density were attributed to a pH-induced conformational and structural change. This indicates d that a compact CRP monolayer was obtained, accompanied by a sharp decrease in thickness as the pH decreased from 7.0 to 4.0 (Fig. 4). When the pH value was lowered to 2.0, the CRP was resolved into a 4.48 ± 0.81 nm thickness and 0.331 ± 0.095 g/cm^3 layer density. Compared with the conformation at pH 6.0, the thickness and layer density decreased 0.27 nm and 0.082 g/cm^3, respectively.

3.7. CRP in alkaline pH conditions

Unlike the structural information in an acidic environment, the conformational change in the structure of CRP in the alkaline region was still unknown in previous reports. The homopentamer CRP was resolved into thicknesses of 1.99 ± 0.18 and 2.20 ± 0.11 nm and layer densities of 0.587 ± 0.084, 0.560 ± 0.088 g/cm^3 at pH 8.0 and 10.0, respectively. These results were similar to the structural parameters at pH 4.0, which indicated that the changes in conformation and structure of CRP may occur or CRP is likely to dissolved as the form of monomer or monomer aggregate in basic environments.

3.8. Dynamic conformational properties of CRP from acidic to basic pH conditions

To probe the dynamic alteration of pH-induced conformation, the CRP monolayer was exposed to various pH solutions. Each of the different solutions with pH from 2.0 to 10.0 reacting with native CRP induced conformational changes, as described above. The thickness (nm) and mass loading (ng/mm^2) of the CRP monolayer after changes under different pH solutions were resolved and are displayed in Fig. 5. The thicknesses of 4.75 ± 0.31 (pH 2.0 changed to pH 7.0), 4.32 ± 0.37 (pH 4.0 changed to pH 7.0), 4.30 ± 0.41 (pH 6.0 changed to pH 7.0), 4.32 ± 0.48 (pH 8.0 changed to pH 7.0), and 4.39 ± 0.47 nm (pH 10.0 changed to pH 7.0) were all lower than the thickness (5.70 ± 0.12 nm) obtained at pH 7.0 and could not be compared to the CRP structure at pH 7.0. It may be attributed to an irreversible change in quaternary structure of CRP. Moreover, the surface concentration of the CRP monolayer was resolved into the similar mass loading values of 1.767 ± 0.235 (pH 2.0 changed to pH 7.0), 1.777 ± 0.239 (pH 4.0 changed to pH 7.0), 1.776 ± 0.239 (pH 6.0 changed to pH 7.0), 1.778 ± 0.243 (pH 8.0 changed to pH 7.0), and 1.782 ± 0.238 ng/mm^2 (pH 10.0 changed to pH 7.0). Even the buffer was changed to pH 7.0, the CRP layer was not considered to be a native pentameric form while a partial rearrangement occurred on the aldehyde-functionalized sensor surface. Also, an irreversible monomeric CRP aggregation reaction could not occur in the immobilized CRP monolayer as proven by less variance in thickness and mass loading. Therefore a stable CRP monolayer has a great potential in recycled experiments, especially in the application of biosensors.

3.9. Significance of The pH-induced conformational changes in the structure of CRP

Although the three-dimensional structure of human pentameric doughnut-shaped CRP has been resolved by X-ray crystallography (Shrive et al., 1996), AFM and DPI (Lin, 2006a), the variety of physiological functions of CRP is quite a puzzle. Investigations have signified the potential role of trivial differences in basal CRP concentration seen in healthy individuals and the relationship to the long-term risk of CVD events (Araujo et al., 2009; Musunuru et al., 2008 and Hingorani et al., 2009). Essentially, CRP was reported to require dissociation from a pentamer to a monomer to exert pro-atherosclerosis effects (Verma et al., 2004). The different conformations of CRP under different pH conditions will be an important issue for explaining the various functions of CRP under certain physiologic and pathologic conditions.

The present study shows that the CRP homopentamer structure dissociates into monomers as the pH shifts toward both acidic and alkaline conditions, but only partial rearrangement of CRP subunits occurs at extremely acidic physiological conditions. The CRP was resolved to be a native pentameric form at pH 6.0. One report indicated that at pH 5.0–7.2, CRP presented a polydisperse system, in which the main component was native pentameric CRP (Blizniukov et al., 2003). The process of conformational changes is predominantly driven by electrostatic interactions on the monolayer plain (Wang and Sui, 2001). The interaction between the positively charged protein molecule and the negatively charged silica waveguide surface would weaken the intra-molecular subunits' interaction and minimize non-specific binding to the sensor surface (Wink et al., 1997). Thus, when the layer density of proteins increased on the aldehyde-functionalized sensor surface, the comparatively stronger intermolecular interaction of each CRP subunit led to dissociation of the pentameric structure. As the pH value decreased, the acidic environment could strengthen the electrostatic interaction, resolve monomeric CRP and thus decrease the layer density at the solid–liquid interface. On the other hand, it was originally proposed that the acid-denatured CRP monolayer would be thinner than others. However, the sharp increase in thickness from that at pH 4.0 was probably caused by the hydrophobic residues of monomeric CRP. The hydrophobic affinity induced "partial" subunit aggregation and might have diffused to form a double layer on the aldehyde-functionalized sensor surface (Wu et al., 2002). Our studies show that the pentameric CRP might resolve into monomer at pH 8.0 and 10.0. The conceivable explanation is the disruption of salt bridges among the pentagonal doughnut-shaped structure, which are formed by the $-COO^-$ and $-NH_2$ groups owing the intra-molecular hydrogen bonding under alkaline conditions.

4. Conclusions

The current work revealed that the conformational changes in the structure of the CRP monolayer in acidic regions had two forms, the monomeric CRP, at pH 4.0 and a "partial" subunit aggregation at pH 2.0. On the other hand, only the compact monomeric form was observed in pH 8.0 and 10.0 alkaline regions. Our experiments explore the potential roles of pH-associated CRP conformational changes, which may shed new light on the essential role of CRP in human CVD and metabolic syndrome.

Acknowledgements

This study was supported by grants from the National Science Council (NSC96-2221-E-002-257-MY3, NSC98-2314-B-002-099MY3, NSC98-2320-B-002-006-MY3, NSC98-3114-B-002-001).

References

Araujo, J.P., Lourenco, P., Azevedo, A., Frioes, F., Rocha-Goncalves, F., Ferreira, A., Bettencourt, P., 2009. J. Card. Fail. 15 (3), 256–266.
Arwin, H., 2000. Thin Solid Films 377/378, 48–56.
Blake, G.J., Rifai, N., Buring, J.E., Ridker, P.M., 2003. Circulation 108 (24), 2993–2999.
Blizniukov, O.P., Kozmin, L.D., Falikova, V.V., Martynov, A.I., Tishchenko, V.M., 2003. Biofizika 48 (5), 844–852.
Boncler, M., Watala, C., 2009. Acta Biochim. Pol. 56 (1), 17–31.
Casas, J.P., Shah, T., Hingorani, A.D., Danesh, J., Pepys, M.B., 2008. J. Intern. Med. 264 (4), 295–314.
Davis, F., Higson, S.P., 2005. Biosens. Bioelectron. 21 (1), 1–20.
Devaraj, S., Singh, U., Jialal, I., 2009. Curr. Opin. Lipidol. 20 (3), 182–189.
Hage, F.G., Szalai, A.J., 2009. Curr. Atheroscler. Rep. 11 (2), 124–130.
Hingorani, A.D., Shah, T., Casas, J.P., Humphries, S.E., Talmud, P.J., 2009. Clin. Chem. 55 (2), 239–255.
Khreiss, T., Jozsef, L., Potempa, L.A., Filep, J.G., 2004. Circulation 109 (16), 2016–2022.
Laurent, P., Potempa, L.A., Gewurz, H., Fiedel, B.A., Allen, R.C., 1983. Electrophoresis 4, 316–317.
Lin, S., Lee, C.K., Wang, Y.M., Huang, L.S., Lin, Y.H., Lee, S.Y., Sheu, B.C., Hsu, S.M., 2006a. Biosens. Bioelectron. 22 (2), 323–327.
Lin, S., Lee, C.K., Lin, Y.H., Lee, S.Y., Sheu, B.C., Tsai, J.C., Hsu, S.M., 2006b. Biosens. Bioelectron. 22 (2), 715–721.
Mazer, S.P., Rabbani, L.E., 2004. J. Thromb. Thrombolysis 17 (2), 95–105.
Meyer, H.F., Hartmann, M., Keusgen, M., 2006. Biosens. Bioelectron. 21, 1987–1990.
Musunuru, K., Kral, B.G., Blumenthal, R.S., Fuster, V., Campbell, C.Y., Gluckman, T.J., Lange, R.A., Topol, E.J., Willerson, J.T., Desai, M.Y., Davidson, M.H., Mora, S., 2008. Nat. Clin. Pract. Cardiovasc. Med. 5 (10), 621–635.
Nakou, E.S., Liberopoulos, E.N., Milionis, H.J., Elisaf, M.S., 2008. Curr. Vasc. Pharmacol. 6 (4), 258–270.
Pepys, M.B., Hirschfield, G.M., 2003. J. Clin. Invest. 111 (12), 1805–1812.
Shrive, A.K., Cheetham, G.M., Holden, D., Myles, D.A., Turnell, W.G., Volanakis, J.E., Pepys, M.B., Bloomer, A.C., Greenhough, T.J., 1996. Nat. Struct. Biol. 3 (4), 346–354.
Swann, M.J., Peel, L.L., Carrington, S., Freeman, N.J., 2004. Anal. Biochem. 329 (2), 190–198.
Verma, S., Szmitko, P.E., Yeh, E.T., 2004. Circulation 109 (16), 1914–1917.
Wang, H.W., Sui, S., 2001. J. Struct. Biol. 134 (1), 46–55.
Wen, J., Arakawa, T., 2000. Anal. Biochem. 280 (2), 327–329.
Wink, T., van Zuilen, S.J., Bult, A., van Bennkom, W.P., 1997. Analyst 122 (4), 43R–50R.
Wu, Y., Ji, S.R., Wang, H.W., Sui, S.F., 2002. Biochemistry (Mosc) 67 (12), 1377–1382.